Neuron
Article

Transsynaptic Signaling by Activity-Dependent Cleavage of Neuroligin-1

Rui T. Peixoto,[1,3] Portia A. Kunz,[4] Hyungbae Kwon,[5,6] Angela M. Mabb,[4] Bernardo L. Sabatini,[5] Benjamin D. Philpot,[4] and Michael D. Ehlers[1,2,*]

[1]Department of Neurobiology, Duke University Medical Center, Durham, NC 27710, USA
[2]Pfizer Worldwide Research and Development, Neuroscience Research Unit, Cambridge, MA 02139, USA
[3]Gulbenkian PhD Program in Biomedicine, P-2781-901 Oeiras, Portugal
[4]Department of Cell and Molecular Physiology, Neuroscience Center, Carolina Institute for Developmental Disabilities, University of North Carolina, Chapel Hill, NC 27599, USA
[5]Howard Hughes Medical Institute, Department of Neurobiology, Harvard Medical School, Boston, MA 02115, USA
[6]Present address: Max Planck Florida Institute, Rm 2243, One Max Planck Way, Jupiter, FL 33458, USA
*Correspondence: michael.ehlers@pfizer.com
http://dx.doi.org/10.1016/j.neuron.2012.07.006

SUMMARY

Adhesive contact between pre- and postsynaptic neurons initiates synapse formation during brain development and provides a natural means of transsynaptic signaling. Numerous adhesion molecules and their role during synapse development have been described in detail. However, once established, the mechanisms of adhesive disassembly and its function in regulating synaptic transmission have been unclear. Here, we report that synaptic activity induces acute proteolytic cleavage of neuroligin-1 (NLG1), a postsynaptic adhesion molecule at glutamatergic synapses. NLG1 cleavage is triggered by NMDA receptor activation, requires Ca^{2+}/calmodulin-dependent protein kinase, and is mediated by proteolytic activity of matrix metalloprotease 9 (MMP9). Cleavage of NLG1 occurs at single activated spines, is regulated by neural activity in vivo, and causes rapid destabilization of its presynaptic partner neurexin-1β (NRX1β). In turn, NLG1 cleavage depresses synaptic transmission by abruptly reducing presynaptic release probability. Thus, local proteolytic control of synaptic adhesion tunes synaptic transmission during brain development and plasticity.

INTRODUCTION

Neuronal synapses are maintained by a complex network of adhesion molecules that span the synaptic cleft and juxtapose the presynaptic active zone with the postsynaptic density (Dalva et al., 2007). The tight association between pre- and postsynaptic elements has long suggested that changes on either side of the synapse are transmitted *trans* synaptically (Lisman and Harris, 1993). Indeed, postsynaptic receptor blockade augments presynaptic function through unknown mechanisms (Burrone et al., 2002; Murthy et al., 2001; Thiagarajan et al., 2005; Wierenga et al., 2006), whereas increased activity in dendritic segments retrogradely dampens release probability of contacting presynaptic terminals (Branco et al., 2008). Given their confined localization at synapses and restricted number of interactions, postsynaptic adhesion molecules offer the potential for tight local control over presynaptic function (Futai et al., 2007; Gottmann, 2008; Ko et al., 2009; Missler et al., 2003; Restituito et al., 2011; Stan et al., 2010). However, whether transsynaptic adhesion acutely regulates synapse function is unclear.

Neuroligins (NLGs) are postsynaptic adhesion molecules that bind presynaptic neurexins (NRXs) with nanomolar affinity (Südhof, 2008). Rodents have four NLG isoforms, each exhibiting a specific expression pattern and subcellular distribution. In particular, NLG1 and NLG2 are localized to excitatory and inhibitory synapses, respectively (Graf et al., 2004). NLGs and NRXs contain intracellular domains that interact with scaffold proteins, such as PSD95 and CASK (Südhof, 2008). Adhesion between NLGs and NRXs thus provides a structural bridge between pre- and postsynaptic scaffolding machinery. In humans, NRXs and NLGs have been strongly linked to autism spectrum disorders, emphasizing the importance of this transsynaptic complex for normal brain development (Südhof, 2008). Indeed, NLGs induce functional maturation of presynaptic terminals (Dean et al., 2003; Scheiffele et al., 2000; Wittenmayer et al., 2009), whereas NRXs cluster postsynaptic proteins (Graf et al., 2004; Heine et al., 2008).

Their ability to transaggregate synaptic components implicated NLGs and NRXs as critical mediators of synapse formation. This hypothesis was supported by in vitro studies showing that NLG levels correlate with the number of synapses generated during development (Chih et al., 2005; Dean et al., 2003; Graf et al., 2004; Levinson et al., 2005). However, NLG1-NLG3 triple knockout (KO) neurons exhibit normal synapse number and ultrastructural synaptic features, but present severe deficits in synaptic transmission (Varoqueaux et al., 2006), indicating that, in vivo, NLGs are not required for the initial stages of synaptogenesis, but are critical for proper synaptic function. Recent studies have further shown that NLGs regulate NMDA (Chubykin et al., 2007; Jung et al., 2010) and AMPA (Etherton et al., 2011;

Heine et al., 2008; Shipman et al., 2011) receptor function and are involved in multiple forms of synaptic plasticity across species (Choi et al., 2011; Jung et al., 2010).

Interestingly, overexpression of NLG1 in hippocampal slices and cultured neurons increases release probability through NRX-dependent mechanisms (Futai et al., 2007; Ko et al., 2009; Stan et al., 2010), whereas disruption of endogenous NLG-NRX interactions with soluble Fc-NRX fragments decreases miniature excitatory postsynaptic current (mEPSC) frequency and release probability (Levinson et al., 2005). In vivo, transgenic expression of NLG1 results in extended active zones and increased number of reserve pool vesicles (Dahlhaus et al., 2010), while neurons lacking αNRX1-αNRX3 exhibit deficits in synaptic transmission due to impaired N-type Ca^{2+} channel function (Missler et al., 2003). These results suggest that the NLG-NRX transsynaptic complex is an important regulator of presynaptic function. However, a limitation of most studies to date is the reliance on long-term manipulations susceptible to indirect compensatory mechanisms. High frequency stimulation of cultured hippocampal neurons induces fast morphological changes of NLG1 puncta (Gutiérrez et al., 2009), indicating that NLG1 can be acutely regulated by activity. Yet, the underlying mechanisms, activity-dependent signals, and functional consequences of acute NLG1 regulation at synapses remain unknown.

MMPs are a large family of secreted Zn^{2+}-dependent proteolytic enzymes that cleave extracellular matrix components and pericellular proteins. MMP2, MMP3, and MMP9 are highly abundant in the brain and have been associated with synaptogenesis, synaptic plasticity, and multiple neuropathological conditions (Ethell and Ethell, 2007; Yong, 2005). In particular, MMP9 is acutely upregulated and secreted in response to neuronal activity and is required for the expression of long-term potentiation (Bozdagi et al., 2007; Nagy et al., 2006; Wang et al., 2008). Moreover, MMP9 activity is increased following epileptic seizures in the hippocampus and is required for postseizure synaptic plasticity and circuit remodeling (Szklarczyk et al., 2002; Wilczynski et al., 2008). Despite a well-documented role in regulating synapse function and plasticity (Bozdagi et al., 2007; Michaluk et al., 2009; Nagy et al., 2006), the substrates of MMP9 associated with functional remodeling of glutamatergic synapses remain unclear.

In the present study, we demonstrate that synaptic activity triggers rapid MMP9-mediated proteolysis of synaptic NLG1. Cleavage of NLG1 is ubiquitous in the brain, occurs throughout development, and is upregulated by neuronal activity in mature and developing circuits. Using a combination of biochemical, live cell imaging, and electrophysiological analysis, we show that postsynaptic cleavage of NLG1 occurs at single activated dendritic spines, requires NMDA receptor and Ca^{2+}-calmodulin-dependent kinase (CaMK) signaling, and causes rapid destabilization of presynaptic NRX1β. Acute NLG1 cleavage in turn suppresses synaptic strength by rapidly reducing presynaptic release probability. Together, our results indicate that postsynaptic activity influences presynaptic function by NLG1 cleavage, revealing a posttranslational mechanism of NLG1 regulation that contributes to synapse plasticity in vivo. Activity-dependent cleavage of synaptic adhesion complexes may provide a general paradigm for transsynaptic signaling in diverse neural circuits.

RESULTS

Neuronal Activity Induces Rapid Loss of Synaptic NLG1

To determine the effect of neuronal activity on synaptic NLGs, we treated dissociated 21 days in vitro (DIV21) cortical cultures with 30 mM KCl for 2 hr. Endogenous NLG levels were assessed by immunocytochemistry using a pan-NLG antibody directed against the C-terminal domain of NLG1-NLG4. PSD95 immunolabeling was used to identify glutamatergic synapses. Following KCl treatment, pan-NLG levels at PSD95-positive dendritic spines were reduced by 29.5% ± 5.3% relative to control (Figures 1A and 1B). A similar change was observed in total pan-NLG levels (28.9% ± 1.1% decrease after KCl), indicating a net loss of NLGs across the entire cell (Figure 1B). NLG1 predominantly partitions to and regulates glutamatergic synapses (Chubykin et al., 2007; Graf et al., 2004). The loss of NLGs from PSD95-positive sites prompted us to test whether depolarization depletes NLG1 from the postsynaptic density (PSD). Due to the lack of NLG1-specific antibodies suitable for immunocytochemistry, we performed biochemical fractionation of DIV21 cortical cultures after KCl stimulation (Ehlers, 2003) and measured NLG1 levels using an antibody targeted against the extracellular N-terminal domain. Immunoblot analysis of isolated fractions revealed enrichment of NLG1 in the PSD (Figure S1 available online). KCl depolarization resulted in a significant loss (47.6% ± 1.8%) of NLG1 from total extracts (Figures 1C and 1D). This reduction in NLG1 was observed in both synaptic plasma membrane (SPM) and PSD fractions (30.5% ± 1.5% decrease in SPM; 23.9% ± 7.3% in PSDI; 45.1% ± 5.4% in PSDIII) and was particularly pronounced in Triton-insoluble PSDII fractions (72.9% ± 4.9% reduction), in which NLG1 is most highly enriched (Figure S1).

We next tested whether KCl incubation increases NLG1 internalization and lysosomal degradation using surface biotinylation (Ehlers, 2000). To inhibit lysosomal proteolysis, cells were preincubated with leupeptin for 1 hr. In basal conditions, 5.3% ± 1.2% of surface NLG1 was internalized over 2 hr (Figures 1E and 1F). This low internalization rate was unaltered by KCl (5.7% ± 0.8% of surface NLG1 internalized), indicating that KCl-induced NLG1 loss is not due to increased internalization. By contrast, the GluA1 receptor exhibited a marked increase in internalization upon KCl stimulation (Figure 1F, right panel), similar to previous reports (Ehlers, 2000). We further addressed whether KCl-induced loss of total NLG1 was sensitive to proteasome or lysosome inhibition. Incubation with KCl for 2 hr resulted in a 48.1% ± 2.6% reduction of total NLG1 levels, which was unaffected by proteasome inhibition (MG132, 50 μM), blockade of lysosomal degradation (leupeptin, 200 μM), or both together (MG132, 51.5% ± 5.7%; leupeptin, 46.3% ± 6.7%; both, 47.4% ± 4.2% of control; Figures 1G and 1H). However, incubation with the broad-spectrum MMP inhibitor GM6001 (10 μM) abolished KCl-induced loss of NLG1 (102.9 ± 1.1% of control; Figures 1G and 1H), whereas incubation with GM6001, MG132, or leupeptin alone did not significantly alter NLG1 levels under basal conditions (MG132,

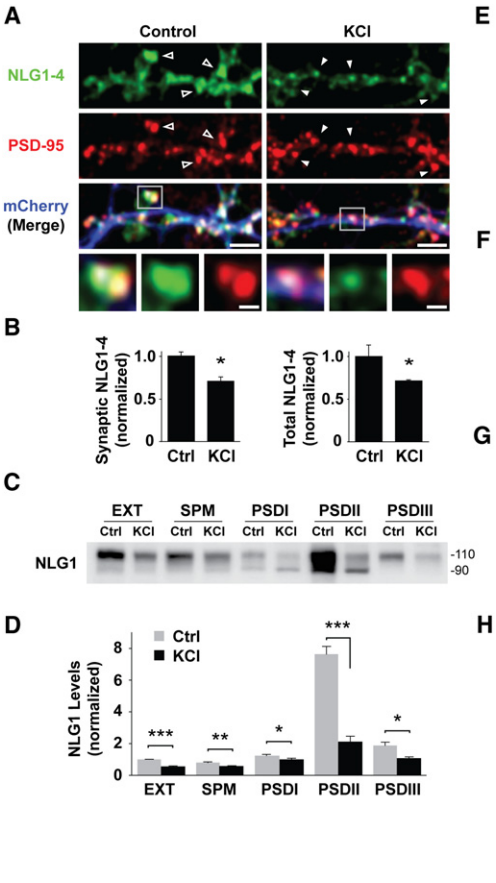

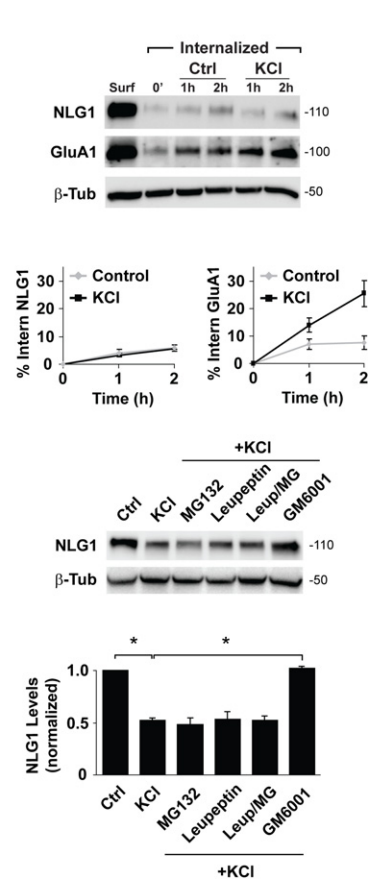

Figure 1. Neuronal Activity Triggers Loss of Neuroligin-1 from Synapses

(A) Hippocampal neurons (DIV21) incubated in media (control) or media with 30 mM KCl for 2 hr (KCl) immunolabeled for PSD95 and pan-NLG (NLG1–NLG4). Arrows show NLG1–NLG4 labeling at PSD95-positive synapses under control conditions (open) or after KCl (solid). Boxed regions are magnified in lower panels. Scale bars, 5 μm and 1 μm.

(B) Means ± SEM of NLG1–NLG4 fluorescence intensity in PSD95-positive spines (left) or entire neurons (right) normalized to controls. Control, n = 435 puncta, 8 neurons; KCl, n = 546 puncta, nine neurons. *p < 0.01.

(C) Immunoblot analysis of NLG1 in membrane fractions isolated from control (Ctrl) or KCl-treated cortical neurons (DIV21). EXT, whole cell extract; SPM, synaptic plasma membrane; PSDI,II, III; postsynaptic density fractions. Note that 4-fold less protein by mass was loaded in PSD fraction lanes. See Experimental Procedures for details.

(D) Means ± SEM of NLG1 protein levels relative to EXT control. n = 3, *p < 0.05, **p < 0.005, ***p < 0.001.

(E) Biotinylation assay of endocytosis performed on DIV21 cortical neurons incubated in media (Ctrl) or media with 30 mM KCl. Surf, total surface protein at time zero. See Experimental Procedures for details.

(F) Quantitative analysis of NLG1 (left) and GluA1 (right) internalization over time.

(G) Immunoblot of NLG1 in lysates of DIV21 cortical cultures following 2 hr incubation in medium (Ctrl) or medium with 30 mM KCl alone or supplemented with MG132 (10 μM), leupeptin (200 μM), leupeptin+MG132 (Leup/MG), or GM6001 (10 μM). Note that GM6001 prevents KCl-induced loss of total NLG1.

(H) Means ± SEM of total NLG1 under indicated conditions. n = 3, *p < 0.05.

See also Figure S1.

103.6% ± 4.4%; leupeptin, 102.1% ± 0.8%; GM6001, 109.8% ± 5.1% of control; Figures S1B and S1C).

Juxtamembrane Cleavage of Neuroligin-1 Releases Its N-Terminal Ectodomain

To test whether NLG1 is cleaved at the plasma membrane, we developed an assay based on surface biotinylation (Figure 2A). Briefly, DIV21 neuronal cultures were covalently labeled with cell impermeable biotin (Sulfo-LC-Biotin-NHS, 1 mg/ml) to exclusively label surface proteins. Following incubation at 37°C, culture media was collected, centrifuged, and incubated overnight with streptavidin beads to isolate released soluble biotin conjugates prior to immunoblot analysis. Using this assay, we detected accumulation of ~90 kDa soluble polypeptide(s) recognized by N-terminal NLG1 antibody in the media (Figure 2B). To control for possible artifacts generated by biotinylation, we filtered media from unbiotinylated neuronal cultures using a 30 kDa cutoff filter, and similar ~90 kDa bands were detected in the concentrated fractions (Figure S2A). Initially postulated as breakdown products (Ichtchenko et al., 1995), ~90 kDa NLG1 species have been widely observed and considered to be immature unglycosylated forms of NLG1 (Ko et al., 2009; Scheiffele et al., 2000). To test whether ~90 kDa NLG1 polypeptide(s) correspond to immature or incompletely glycosylated isoforms, we enzymatically deglycosylated N- and O-linked glycans from media-collected biotinylated fractions and examined electrophoretic mobility. Deglycosylation resulted in equivalent migration shifts of full length and soluble ~90 kDa NLG1 species (Figure 2C), identifying the latter as cleaved NLG1 N-terminal fragments (NLG1-NTFs) rather than immature nonglycosylated species.

To determine if NLG1 is cleaved in vivo, we analyzed soluble fractions of cortical, hippocampal, and cerebellar tissue from adult P60 mice (Figure 2D). Several NLG1 bands of ~90 kDa were present in all brain fractions, indicating that multiple cleavage fragments are generated in vivo. Enzymatic deglycosylation of these fractions also resulted in a migration shift of NLG1-NTFs, indicating that they originate from mature forms of NLG1 (Figures 2E and S2B). To exclude possible antibody nonspecificity, we tested whether similar bands were detected in extracts of NLG1 KO mice (Varoqueaux et al., 2006). Both 110 kDa full form and ~90 kDa NLG1-NTFs were absent in NLG1 KO brain extracts and respective soluble fractions (Figure 2F), confirming that the NTFs detected correspond to

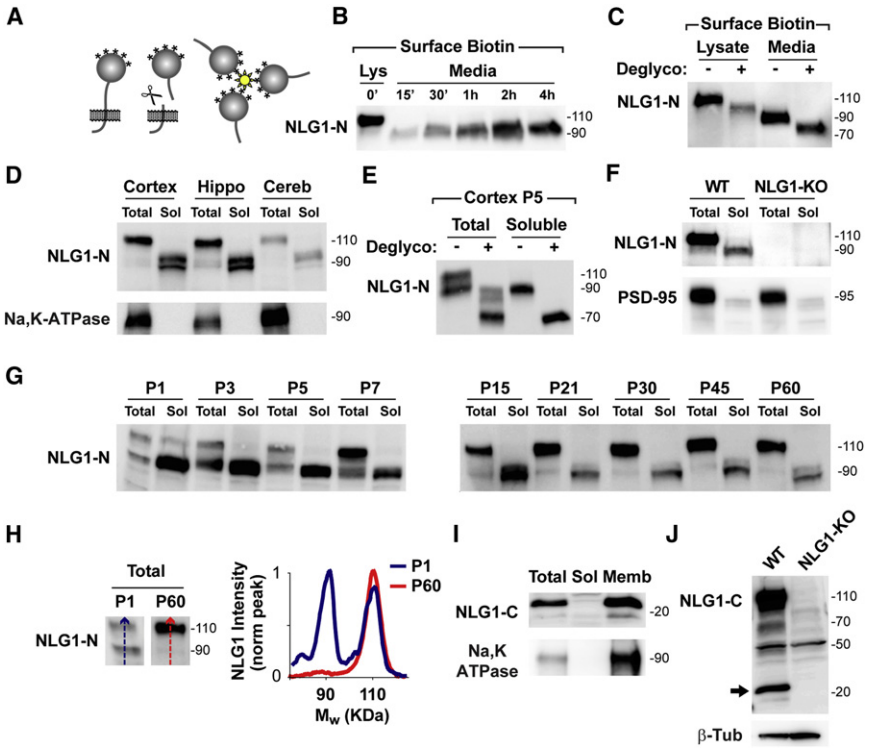

Figure 2. A Soluble N-Terminal Fragment of NLG1 Is Abundant in Brain

(A) Diagram of biotinylation-based cleavage assay. Media from surface biotinylated neuronal cultures was collected and soluble biotin conjugates isolated by streptavidin precipitation.

(B) Immunoblot analysis of NLG1 reveals time-dependent release of soluble ~90 kDa NLG1-NTFs to culture media. Lys, 10% total surface protein at time zero.

(C) Deglycosylation induces an equivalent mass shift of both full-length NLG1 (Lysate) and NLG1-NTFs (Media) collected after surface biotinylation.

(D) Immunoblot analysis of NLG1 in whole homogenates (5 μg, Total) and soluble (50 μg, Sol) fractions obtained from cortical, hippocampal, and cerebellar tissue from P60 WT mice reveals soluble ~90 kDa NLG1-NTFs.

(E) Deglycosylation of whole homogenates (Total) and soluble fractions from P5 WT mouse cortex results in an ~20 kDa apparent mass shift of NLG1-NTFs.

(F) Immunoblot analysis of NLG1 in whole brain homogenates (Total) and soluble fractions (Sol) from WT and NLG1-KO mice reveals absence of NLG1-NTFs in NLG1-KO tissue.

(G) Developmental profile of NLG1-NTFs from WT mouse cortical extracts at different postnatal days (P). Total, 10 μg whole cortical homogenates; Sol, 50 μg soluble fractions.

(H) Line scan analysis of immunoblots shown in (G). Note that the relative abundance of NLG1-NTFs is higher during early developmental stages. The graph plots normalized signal intensity along the lines shown on the blots on the left.

(I) Immunoblot analysis of NLG1-CTFs in total homogenates (Total), soluble fractions (Sol), and membrane fractions (Memb) from P60 WT mouse cortex.

(J) Immunoblot analysis of NLG1-CTFs in whole brain homogenates from WT and NLG1-KO mice reveals the absence of ~20 kDa NLG1-CTFs in NLG1-KO tissue. See also Figure S2.

cleaved NLG1. To characterize the developmental profile of NLG1 cleavage, we performed immunoblot analysis of mouse cortical fractions from birth to adulthood (P1–P60, Figure 2G). Interestingly, NLG1-NTFs are present throughout development and are enriched during the first postnatal week (P1–P7), where they are as abundant as full-length NLG1 (Figures 2G and 2H).

A logical outcome of N-terminal proteolysis is the generation of corresponding intracellular C-terminal fragments (CTFs). Analysis of mouse cortical fractions using an antibody targeted against the C-terminal domain of NLG1 revealed multiple membrane-associated ~20 kDa species, a size consistent with the predicted mass of NLG1-CTFs based on the size of NLG1-NTFs (Figure 2I). These bands are absent in NLG1-KO brain extracts, confirming that they correspond to NLG1 fragments (Figure 2J). To confirm these findings, we expressed a dually tagged version of NLG1 with N-terminal green fluorescent protein (GFP) and C-terminal hemagglutinin (HA) (GFP-NLG1-HA) in COS7 cells. Immunoblot analysis of cell extracts using an anti-HA antibody revealed the presence of ~20 kDa bands in lysates from cells expressing GFP-NLG1-HA, but not GFP-NLG1 (Figure S2C).

Neuronal Activity Induces Cleavage of Neuroligin-1 through an NMDAR-CaMK-MMP9 Signaling Pathway

Combining our biotinylation-based assay with pharmacological manipulation of DIV21 cortical neuron cultures, we assessed how neuronal activity regulates NLG1 cleavage. Whereas preventing action potentials with tetrodotoxin (TTX, 2 μM) decreased NLG1-NTFs (0.65 ± 0.06 of control), increasing network activity with bicuculline (50 μM) and 4-aminopyridine (4AP, 25 μM) significantly increased NLG1 cleavage (Bic/4AP, NLG-NTF levels: 1.5 ± 0.1 of control; Figures 3A and 3B). To mimic conditions that induce robust loss of synaptic NLG1 (Figure 1), we depolarized neurons with 30 mM KCl for 2 hr. Depolarization led to a pronounced increase in NLG1-NTFs (4.4 ± 0.5-fold) compared to control conditions (Figures 3C and 3D). This effect was abrogated by the NMDA receptor antagonist APV (50 μM, 1.0 ± 0.2 of control), whereas APV alone induced no change in NLG1-NTF levels under basal conditions (APV, 0.95 ± 0.1 of control; Figure S3A and S3B). Moreover, brief 5 min incubation with 50 μM NMDA induced a robust increase in NLG1-NTFs, indicating that NMDA receptor activation is both necessary and sufficient to trigger NLG1 cleavage. By contrast, the selective AMPA receptor antagonist NBQX (20 μM) failed to abrogate KCl-induced cleavage (NMDA, 2.4 ± 0.1; KCl+NBQX, 1.92 ± 0.1; NBQX, 1.37 ± 0.1; Figures S3A and S3B). In addition, CaMK inhibitors KN93 (5 μM) and KN62 (10 μM), but not the inactive isomer KN92 (5 μM) also abrogated KCl-induced increase in NLG1-NTFs (KN93, 1.5 ± 0.3; KN62, 1.5 ± 0.4; KN92, 5.0 ± 0.8-fold increase in NLG1-NTFs relative to control; Figures 3C and 3D), indicating that activity-dependent NLG1 cleavage is further regulated by CaMK signaling.

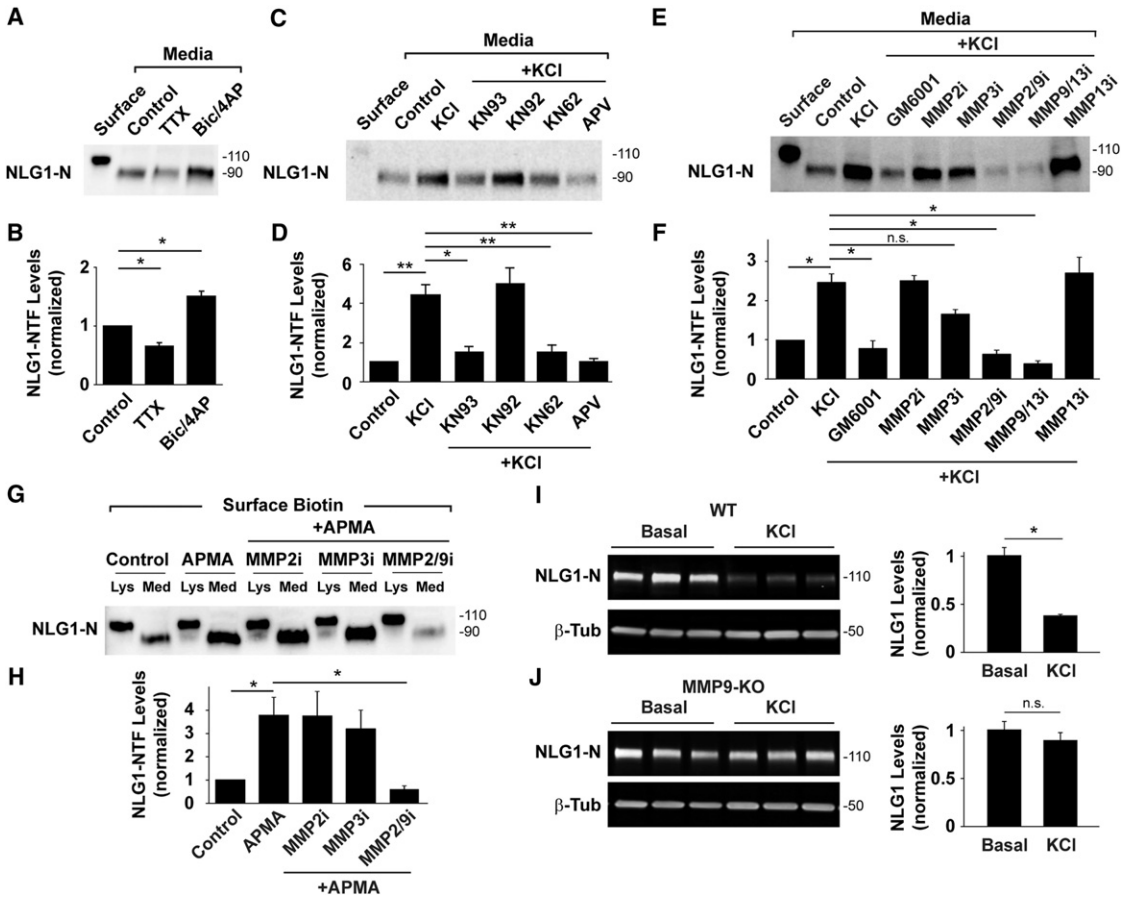

Figure 3. Neuronal Activity Induces NLG1 Cleavage through NMDAR, CaMK, and MMP9 Signaling

(A) Isolation and detection of NLG1-NTFs under control conditions or in the presence of TTX (2 μM) or bicuculline (50 μM) plus 4AP (25 μM, Bic/4AP). Surface, 10% of total surface protein at time zero.

(B) Means ± SEMs of NLG1-NTFs under indicated conditions normalized to control. n = 4, *p < 0.05.

(C) Isolation and detection of NLG1-NTFs under control conditions or in the presence of KCl (30 mM, 2 hr) with or without indicated pharmacological agents.

(D) Means ± SEMs of NLG1-NTFs levels normalized to control. n = 4, *p < 0.05, **p < 0.01.

(E) Isolation and detection of ~90 kDa NLG1-NTFs under control conditions or in the presence of KCl with or without MMP inhibitors. Note that inhibitors targeting MMP9 abrogate KCl-induced NLG1 cleavage.

(F) Means ± SEMs of NLG1-NTFs levels normalized to control. n = 8, *p < 0.005. n.s., not significant.

(G) Immunoblot analysis of NLG1 and NLG1-NTFs in biotinylated fractions of DIV21 cortical neurons treated with the nonselective MMP activator APMA with or without MMP inhibitors. Lys, whole lysates; Med, media. Note that only 10% of precipitate was loaded in Lys lanes.

(H) Means ± SEMs of NLG1-NTFs produced under the indicated conditions normalized to control. n = 3, *p < 0.05.

(I and J) Immunoblot analysis of NLG1 in whole cell extracts from DIV18 cortical neuron cultures from (I) WT or (J) MMP9 KO mice following 2 hr incubation in neurobasal medium (control) or medium with 30 mM KCl (KCl). Bar graphs on the right represent means ± SEM of total NLG1 levels under the indicated conditions for WT (n = 6, *p < 0.01) and MMP9 KO neurons (n = 6, p > 0.05), respectively.

See also Figure S3.

What enzyme is responsible for NLG1 cleavage? Using biotinylation-based isolation of NLG-NTFs, we found that the broad spectrum MMP inhibitor GM6001 (10 μM) prevented activity-induced cleavage of NLG1 (fold increase relative to control: KCl, 2.5 ± 0.2; KCl + GM6001, 0.8 ± 0.2; Figures 3E and 3F). MMP2, MMP3, and MMP9 are the most abundant MMPs in the brain and have been implicated in several forms of synaptic plasticity (Ethell and Ethell, 2007; Yong, 2005). Incubation with MMP2/MMP9 inhibitor II (0.3 μM) or MMP9/MMP13 inhibitor I (20 nM) blocked KCl-induced NLG1 cleavage (NLG1-NTFs relative to control: KCl + MMP2/MMP9i, 0.6 ± 0.1; KCl + MMP9/MMP13i, 0.4 ± 0.1; Figures 3E and 3F). Importantly, the selective MMP2 inhibitor III (50 μM), or MMP13 inhibitor I (0.5 μM) had no significant effect on NLG1 cleavage (NLG1-NTFs relative to control: KCl + MMP2i, 2.5 ± 0.1; KCl + MMP13i 2.7 ± 0.4; Figures 3E and 3F). Interestingly, GM6001, MMP2/MMP9 inhibitor I, and MMP9/MMP13 inhibitor I, but not MMP2 inhibitor III, MMP3 inhibitor III, or MMP13 inhibitor I also reduced NLG1 cleavage under basal conditions (NLG1-NTFs relative to control: GM6001, 0.46 ± 0.09; MMP2i, 0.85 ± 0.13; MMP3i, 0.94 ± 0.13; MMP2/MMP9i, 0.47 ± 0.11; MMP9/MMP13i, 0.27 ± 0.11; MMP13i, 0.92 ± 0.15; Figures S3C and

S3D), indicating that MMP9-dependent cleavage is active not only during periods of elevated neuronal activity, but also under basal conditions. Moreover, we noted that MMP3 inhibitor III (50 μM) induced a partial but nonsignificant decrease in NLG1-NTFs after KCl (KCl + MMP3i, 1.7 ± 0.1, p = 0.092; Figures 3E and 3F). MMPs are secreted as inactive zymogens and require cleavage of their prodomains to become enzymatically active (Ethell and Ethell, 2007). Thus, the effect of MMP3 inhibition could be due to impaired MMP9 activation. To determine which MMP is the terminal protease-cleaving NLG1, we treated neurons with 4-aminophenylmercuric acetate (APMA), a compound that nonselectively activates all MMPs by cleaving their prodomains (Van Wart and Birkedal-Hansen, 1990) and tested the effect of specific MMP inhibitors. Brief incubation of DIV21 cortical neurons with 0.5 mM APMA for 15 min induced robust generation of NLG1-NTFs (3.8 ± 0.8-fold increase relative to control; Figures 3G and 3H). Coincubation with MMP2/MMP9 inhibitor II (0.3 μM) blocked APMA-induced cleavage (0.6 ± 0.1), whereas MMP2 inhibitor III (50 μM) and MMP3 inhibitor III (50 μM) had no effect (3.8 ± 1.0 and 3.2 ± 0.8, respectively), indicating that MMP9 is the downstream protease responsible for cleavage of NLG1. To further validate these findings, we tested how NLG1 is regulated by activity in neurons lacking MMP9. KCl depolarization of DIV17 and DIV18 wild-type (WT) mouse cortical cultures for 2 hr resulted in extensive loss of NLG1 (0.36 ± 0.01 relative to control; Figure 3I). By contrast, KCl incubation of MMP9 KO cultures induced no loss of NLG1 (0.90 ± 0.04 relative to control; Figure 3J), confirming that MMP9 is responsible for activity-dependent regulation of NLG1.

To characterize the activity-dependent production of NLG1-CTFs, we measured CTF levels in whole cell extracts of DIV21 dissociated neuron cultures treated with KCl. As expected, KCl incubation increased NLG1-CTF levels (1.6 ± 0.4 compared to control; Figures S3E and S3F). Interestingly, inhibition of the γ-secretase complex with DAPT (20 μM) during KCl treatment resulted in increased accumulation of NLG1-CTFs (KCl+DAPT, 3.7 ± 0.8; Figures S3E and S3F), indicating that NLG1 is processed by the γ-secretase complex following ectodomain cleavage.

Extracellular Cleavage of NLG1 Occurs Near Its Transmembrane Domain

Deglycosylation of NLG1-NTFs produces ~70 kDa species (Figure 2E), which, based on amino acid mass, indicates that proteolysis occurs in the extracellular juxtamembrane region of NLG1. To determine the specific domain targeted for cleavage, we generated a series of mutants with sequential deletions and amino acid (aa) replacements in the juxtamembrane domain (Figure 4A). NLG1 mutants were screened for their resistance to APMA cleavage using biotinylation-based labeling and isolation of NLG1-NTFs in COS7 cells. Brief incubation with APMA resulted in robust shedding of GFP-NLG1 (Figure 4B). This effect was blocked by GM6001, confirming that MMPs cleave NLG1 under these conditions (Figure 4B). Substituting 60 aa of the NLG1 stalk domain (aa 636–695) with the polylinker GAAAAA resulted in a mutant (NLG1-ΔSDfull) that is resistant to APMA (Figures 4A and 4B). Within this 60 residue stretch, deletion of aa 672–695 (NLG1-ΔSD3) and replacement with the polylinker GAAAAA likewise abolished APMA-induced cleavage, whereas mutation of more membrane-distal sequences did not (aa 636–660, NLG1-ΔSD1; aa 654–677, NLG1-ΔSD2). Notably, we attempted to further resolve the precise cleavage site, but shorter deletions or single site mutants were all cleaved upon APMA treatment, potentially due to the presence of multiple MMP target sequences within this domain. Importantly, the ΔSD3 mutation does not alter NLG1 localization, as GFP-NLG1-ΔSD3 exhibited a similar distribution pattern and synaptic enrichment as wild-type GFP-NLG1 when expressed in DIV21 hippocampal neurons (Figure S4A). Moreover, GFP-NLG1-ΔSD3 and GFP-NLG1 induced quantitatively similar spine formation when expressed in mouse cortical neurons in vivo from E15.5 to P17 and P18, indicating that GFP-NLG1-ΔSD3 retains the synaptogenic properties of wild-type NLG1 (Figures S4D and S4E). To address if NLG1-ΔSD3 is resistant to activity-dependent cleavage in neurons, we tested the effect of KCl depolarization in neurons expressing GFP-NLG1 and GFP-NLG1-ΔSD3. Following 2 hr of KCl incubation, synaptic GFP-NLG1 fluorescence decreased to 55.9% ± 5.4% of initial value, whereas GFP-NLG1-ΔSD3 exhibited no change upon KCl treatment (101.9% ± 6.9% of initial fluorescence level; Figures S4A and S4B).

Rapid Cleavage of NLG1 in Dendritic Spines Following Local Glutamate Uncaging

To address if NLG1 cleavage occurs locally in response to increased synaptic activity, we released glutamate at single dendritic spines by two-photon laser-induced photolysis of (4-methoxy-7-nitroindolinyl)-glutamate (MNI-glutamate), while imaging dendrites of neurons expressing GFP-NLG1-WT or GFP-NLG1-ΔSD3 (Figures 4C–4L). Analysis was performed in CA1 pyramidal neurons in organotypic hippocampal slices at a time corresponding to P14 with tdTomato (tdT) coexpression used as a cell fill. Stimulation near (~1 μm) the distal head of a dendritic spine (Spine 1) with 80 4-ms laser pulses at 2 Hz induced rapid loss of spine GFP-NLG1 within 1 min, whereas no change in fluorescence was detected in the neighboring dendritic shaft (ΔGFP/tdT: Spine 1: 0.61 ± 0.04, dendrite: 1.01 ± 0.02; Figures 4C, 4F, and 4J). We observed a smaller, partial loss of NLG1-GFP in neighboring spines (Spine 2, ΔGFP/tdT: 0.79 ± 0.15), possibly due to the diffusion of intracellular signals. Incubation with the MMP2/MMP9 inhibitor II (0.3 μM) or GM6001 (10 μM) abrogated glutamate-induced GFP-NLG1 loss (MMP2/MMP9i: ΔGFP/tdT: Spine 1, 0.89 ± 0.10; Spine 2, 0.97 ± 0.12; dendrite, 0.98 ± 0.11; Figures 4D, 4G, and 4K; GM6001: ΔGFP/tdT: Spine 1, 0.91 ± 0.04; dendrite, 0.96 ± 0.03; Figures S4F–S4H). Moreover, the cleavage resistant GFP-NLG1-ΔSD3 was unaffected by glutamate uncaging (ΔGFP/tdT: Spine 1, 0.99 ± 0.05; Spine 2, 0.96 ± 0.11; dendrite, 1.05 ± 0.04; Figures 4E, 4H, and 4L).

Cleavage of NLG1 Destabilizes Presynaptic Neurexin-1β

To address how NLG1 cleavage affects synaptic function, we developed a system to acutely and selectively cleave NLG1 on demand (Figure 5A; Movie S1). For this, we inserted the thrombin (Thr) proteolytic recognition sequence LVPRGS into the stalk domain of NLG1 downstream of the dimerization

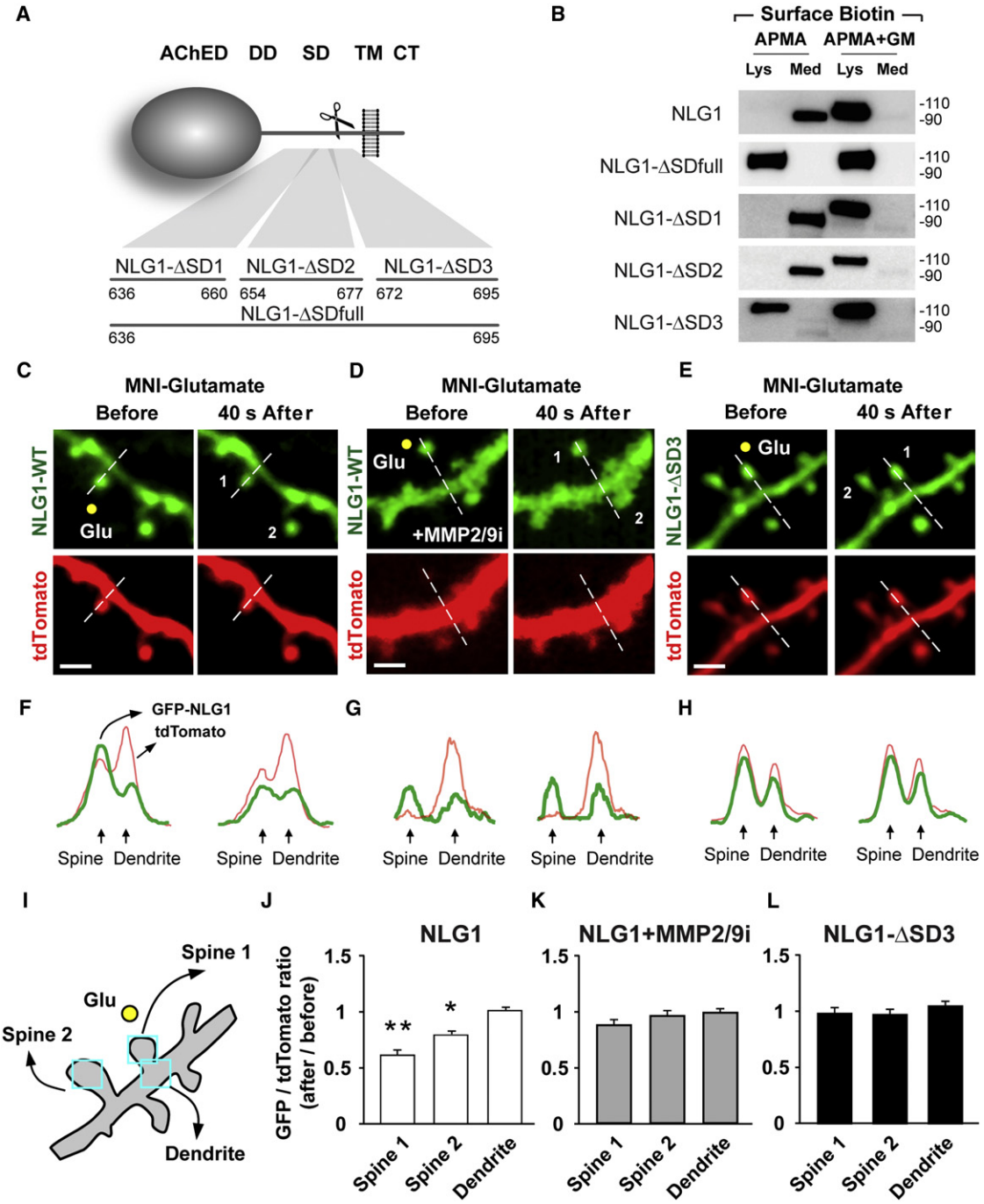

Figure 4. Local Glutamate Uncaging Triggers Rapid Cleavage of Synaptic NLG1

(A) Model illustrating the NLG1-ΔSD substitution mutants in relation to NLG1 domains. AChED, acetylcholinesterase homology domain; DD, dimerization domain; SD, stalk domain; TM, transmembrane domain; CT, C-terminal domain. Numbers indicate amino acids.

(B) Biotinylation-based cleavage assay of COS7 cells expressing the indicated NLG1 mutants. Total lysates (Lys) or media (Med) were collected and subjected to immunoblot analysis following treatment with the MMP activator APMA with or without the broad spectrum MMP inhibitor GM6001 (GM). Both NLG1-ΔSDfull and NLG-ΔSD3 were resistant to APMA-induced cleavage, indicating that MMP cleavage sites lie between residues 672 and 695.

(C) Time-lapse images of hippocampal neurons expressing GFP-NLG1 and tdTomato before and after glutamate uncaging. The yellow dot represents the uncaging spot. "1" represents the dendritic spine stimulated with glutamate and "2" represents a neighboring spine within 10 μm of spine 1. Dashed white line represents the contour used for fluorescence analysis in (F). Scale bars, 2 μm.

(D) Same as (C), but glutamate uncaging was performed in the presence of MMP2/MMP9 inhibitor II (0.3 μM). Scale bar, 2 μm.

(E) Same as (C), but cells express GFP-NLG1-ΔSD3 and tdTomato. Scale bar, 2 μm.

domain, replacing the endogenous sequence TTTKVP. In these experiments, the NLG1ΔA splice variant lacking splice site A was chosen, due to its stringent partitioning into excitatory synapses (Chih et al., 2006). This Thr-cleavable mutant (GFP-Thr-NLG1) localized to synapses in a manner indistinguishable from wild-type GFP-NLG1 in DIV21 hippocampal neurons (Figures 5A–5D). Incubation with 5 U/ml Thr for 30 min resulted in rapid and extensive reduction of GFP-Thr-NLG1 synaptic fluorescence (fractional fluorescence remaining; 0.20 ± 0.03; Figures 5A–5G; Movie S1). Control neurons transfected with GFP-NLG1 lacking a Thr recognition sequence exhibited no change in GFP fluorescence upon Thr treatment (fractional fluorescence remaining; 0.99 ± 0.02; Figure 5H; Movie S2 right panel), indicating that the reduced GFP fluorescence was not due to photobleaching. To determine how acute NLG1 shedding affects postsynaptic morphology and integrity, we co-transfected neurons with mCherry (mCh) or PSD95-mCh and compared fluorescence changes after 30 min of Thr incubation. No significant changes in spine volume measured by the mCh cell fill (mCh fluorescence ratio post/prethrombin; 1.04 ± 0.03; Figures 5A and 5F; Movie S1) or PSD95-mCh puncta intensity (PSD95-mCh fluorescence ratio post/prethrombin; 0.97 ± 0.02; Figures 5B and 5F) were detected after Thr treatment.

To test whether acute cleavage of NLG1 regulates presynaptic NRX1β, we sequentially transfected neuronal cultures with GFP-Thr-NLG1 and NRX1β-mCh lacking splice site 4, obtaining distinct populations of neurons expressing each construct. This approach generated pre- and postsynaptic pairs labeled with NRX1β-mCh and GFP-Thr-NLG1, respectively. At dually labeled synapses, acute Thr treatment caused a rapid and pronounced decrease in NRX1β-mCh fluorescence (Figures 5E–5G; Movie S2; fractional fluorescence remaining: 0.51 ± 0.04). Further analysis of the kinetics of GFP-Thr-NLG1 and NRX1β-mCh level at a higher sampling rate revealed that loss of both proteins occurs in tandem (Figures S5A–S5D). Importantly, there was no detectable change in presynaptic synaptophysin-mCh signal intensity (fractional fluorescence remaining: 0.99 ± 0.08) under similar conditions (Figures 5D and 5F), indicating that destabilization of NRX1β by NLG1 cleavage is specific and not due to indirect structural changes in presynaptic terminals. This was further confirmed by immunolabeling of the vesicular glutamate transporter VGLUT1, which was unaffected by acute NLG1 cleavage (Figures S5E–S5G).

NLG1 Cleavage Decreases Synaptic Strength by Reducing Presynaptic Release

To define the physiological effects induced by acute NLG1 cleavage, we used whole-cell electrophysiological recordings to measure synaptic transmission on DIV15–DIV25 hippocampal neurons expressing GFP-Thr-NLG1 for 3–5 days. This system allowed us to monitor synaptic transmission in the same neuron before and after selective Thr-induced cleavage of NLG1. Recordings from neurons expressing GFP-NLG1 lacking a Thr cleavage site were used to control for possible off-target effects of Thr activity. We first examined the effect of NLG1 cleavage on miniature excitatory postsynaptic currents (mEPSCs; Figure 6A). Application of Thr for 30 min reduced mEPSC frequency (44% ± 10% of baseline; Figures 6B and S6A) with no significant effect on amplitude (91% ± 8% of baseline; Figures 6C and S6A), indicating that NLG1 ectodomain cleavage does not change postsynaptic AMPA receptor number or function, but rather reduces neurotransmitter release or decreases the number of functional excitatory synapses. By contrast, Thr had no effect on mEPSCs in neurons expressing GFP-NLG1 (mEPSC frequency, 100% ± 3% of baseline; amplitude, 102% ± 4% of baseline; Figures 6A–6C and S6B). Importantly, there was no difference in baseline mEPSCs between neurons expressing GFP-NLG1 (frequency: 1.74 ± 0.44 s^{-1}; amplitude: 11.66 ± 1.70 pA) and GFP-Thr-NLG1 (frequency: 2.00 ± 0.36 s^{-1}; amplitude: 10.74 ± 0.61 pA). Consistent with the predominant localization of NLG1 to glutamatergic synapses (Chubykin et al., 2007; Graf et al., 2004), NLG1 cleavage failed to alter miniature inhibitory postsynaptic current (mIPSC) frequency or amplitude (mIPSC frequency: 103 ± 3%; mIPSC amplitude: 98% ± 8% of baseline; Figures S6C–S6F), indicating that NLG1 cleavage does not acutely alter GABAergic transmission.

The reduction in mEPSC frequency (Figures 6A, 6B, and S6A) together with the destabilization of NRX1β (Figures 5C–5G) suggested a possible alteration in presynaptic function. To test this further, we examined the effects of Thr-induced NLG1 cleavage on evoked excitatory synaptic currents (eEPSCs) and their paired-pulse responses. Evoked responses were elicited by stimulating nearby cells with an interstimulus interval of 100 ms. Neurons expressing GFP-NLG1 or GFP-Thr-NLG1 exhibited similar baseline paired-pulse ratio (PPR) responses (GFP-NLG1: 1.42 ± 0.12; GFP-Thr-NLG1: 1.59 ± 0.46). Recordings were then made on the same cell before and 30 min after thrombin application. Thrombin treatment of neurons expressing GFP-Thr-NLG1 reduced the amplitude of the first response and increased PPR (eEPSC amplitude: 50% ± 18% of baseline; PPR: 139% ± 8% of baseline; Figures 6D–6F), strongly suggesting that NLG1 cleavage decreases the probability of neurotransmitter release. This effect was not attributable to Thr treatment per se, as there was no change in eEPSC amplitude or PPR in neurons expressing GFP-NLG1 lacking a Thr cleavage sequence (eEPSC amplitude: 95% ± 8% of baseline; PPR: 106% ± 6% of baseline; Figures 6D–6F).

To address whether specific blockade of NLG1 cleavage also alters release probability, we expressed GFP-NLG1 or GFP-NLG1-ΔSD3 in DIV17 hippocampal neurons and

(F–H) Fluorescence intensity profiles of GFP (green) and tdTomato (red) along the white dashed lines depicted in (C–E).
(I) Representation of the dendrite segment depicted in (E), illustrating analysis of GFP and tdTomato fluorescence in dendritic spines and adjacent dendritic shaft regions.
(J–L) Means ± SEMs of GFP/tdTomato fluorescence intensity ratio after glutamate uncaging in dendritic spines and adjacent dendritic shaft regions in the conditions represented in (C–E), respectively. n = 10, 11, and 11; *p < 0.05, **p < 0.001.
See also Figure S4.

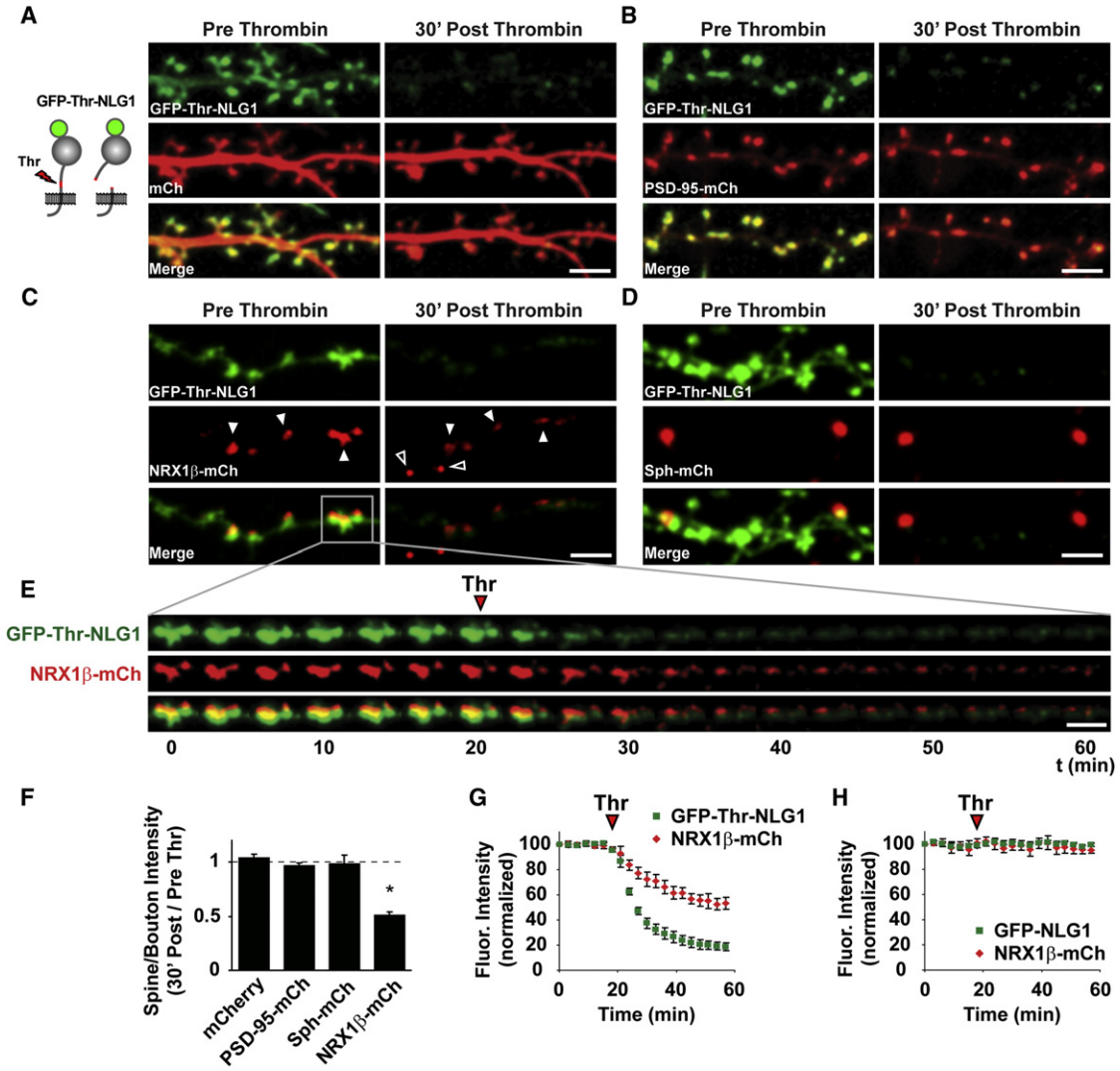

Figure 5. Juxtamembrane Cleavage of Neuroligin Destabilizes Presynaptic Neurexin-1β

(A) Left, schematic of thrombin-cleavable NLG1. Right, DIV21 hippocampal neurons expressing GFP-Thr-NLG1 and mCherry for 3–5 days were imaged before (Pre) and 30 min after (Post) thrombin incubation. Scale bar, 5 μm.

(B) Same as (A), but neurons expressed GFP-Thr-NLG1 and PSD95-mCh. Scale bar, 5 μm.

(C) Dually labeled synapses with postsynaptic GFP-Thr-NLG1 and presynaptic NRX1β-mCh imaged by confocal microscopy before (Pre) and 30 min after (Post) thrombin incubation. Solid arrowheads show loss of presynaptic NRX1β-mCh apposed to postsynaptic GFP-Thr-NLG1 puncta. Open arrowheads show generation of mobile NRX1β-mCh puncta along the axon. Scale bar, 5 μm.

(D) Same as (C), but cells were cotransfected with GFP-Thr-NLG1 and synaptophysin-mCh (Sph-mCh). Sph-mCh is not affected GFP-Thr-NLG1 cleavage. Scale bar, 5 μm.

(E) Time lapse of the highlighted region depicted in (C). The red arrowhead shows the time of thrombin (Thr) application. Scale bar, 5 μm.

(F) Means ± SEM of fluorescence intensity change 30 min after thrombin (Thr) cleavage at synapses expressing GFP-Thr-NLG1. mCherry, n = 307 spines; PSD95-mCh, n = 403 spines; Sph-mCh, n = 43 synaptic pairs; NRX1β-mCh, n = 87 synaptic pairs, *$p < 0.05$.

(G) Fluorescence intensity before and after thrombin application at synapses containing presynaptic NRX1β-mCh and postsynaptic GFP-Thr-NLG1. Arrowhead shows time of thrombin (Thr) application. n = 87 synaptic pairs.

(H) Same as (G), but neurons expressed GFP-NLG1 lacking a thrombin cleavage site. n = 76 synaptic pairs.

See also Figure S5 and Movies S1 and S2.

compared FM4-64 unloading kinetics from contacting presynaptic terminals at DIV21 (Figures 6G–6I). To increase basal rate of NLG1 cleavage, cultures were incubated with bicuculline (50 μM) and 4AP (25 μM) 2 days prior to imaging (Figures 3A and 3B). Interestingly, terminals apposing synapses with GFP-NLG1-ΔSD3 exhibited faster FM4-64 unloading kinetics (τ = 46.1 ± 1.2 s; Figure 6G) than terminals contacting GFP-NLG1-expressing cells (τ = 60.5 ± 1.5 s), indicating that blocking NLG1 cleavage increases presynaptic release probability.

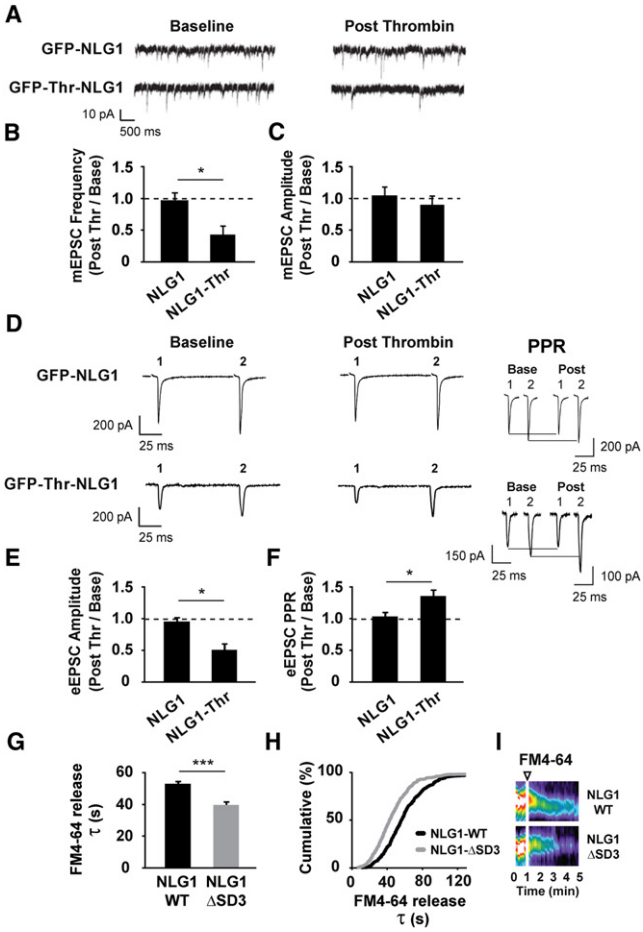

Figure 6. NLG1 Cleavage Rapidly Reduces Release Probability at Excitatory Synapses

(A) Miniature EPSCs (mEPSCs) recorded before (Baseline) and 30 min after (Post) thrombin treatment in hippocampal neurons (DIV15–DIV25), expressing GFP-Thr-NLG1 or GFP-NLG1.

(B) Means ± SEM of mEPSC frequency and (C) amplitude change after thrombin incubation in neurons expressing GFP-NLG1 or GFP-Thr-NLG1. n = 8 and 5 for GFP-Thr-NLG1 and GFP-NLG1, respectively. *$p < 0.01$.

(D) Paired-pulse EPSCs recorded before (Baseline) or 30 min after (Post) thrombin treatment in hippocampal neurons (DIV15–DIV25), expressing GFP-Thr-NLG1 or GFL-NLG. Insets depict traces before and after thrombin treatment, normalized to the amplitude of the first excitatory postsynaptic potential.

(E) Means ± SEM of eEPSC amplitude change after thrombin in neurons expressing GFP-NLG1 or GFP-Thr-NLG1. n = 6 and 6; *$p < 0.05$.

(F) Means ± SEM of paired-pulse ratio change after thrombin in neurons expressing GFP-NLG1 or GFP-Thr-NLG1. n = 6 and 6; *$p < 0.05$.

(G) Means ± SEM of time constants (τ) from stimulus-induced FM4-64 fluorescence decay measurements in presynaptic terminals apposing neurons expressing GFP-NLG1 or GFP-NLG1-ΔSD3. Terminals apposing GFP-NLG1-ΔSD3 synapses exhibit faster FM4-64 decay kinetics. GFP-NLG1-ΔSD3, n = 396 terminals, 12 neurons; GFP-NLG1, n = 438 terminals, 11 neurons; ***$p < 0.0001$.

(H) Cumulative distribution of FM4-64 decay constants (τ) of terminals analyzed in (G).

(I) Representative kymographs of FM4-64 intensity in terminals apposing GFP-NLG1 or GFP-NLG1-ΔSD3. Arrowhead indicates time of KCl application. See also Figure S6.

NLG1 Is Cleaved by MMP9 in Response to Increased Neuronal Activity in Mature and Developing Circuits

To address whether cleavage of NLG1 is regulated by activity in vivo, we measured NLG1-NTFs generated during pilocarpine-induced status epilepticus (PSE) in mice. Intraperitoneal administration of pilocarpine in P60 mice induced robust seizures and resulted in a 2.2 ± 0.3-fold increase of soluble NLG1-NTFs in the hippocampus after 2 hr PSE (Figures 7A–7C). To test whether MMP9 is involved in PSE-induced NLG1 cleavage, we performed pilocarpine injections in MMP9 KO mice. Notably, 2 hr PSE characterized by robust behavioral seizures failed to elevate soluble NLG1-NTFs in MMP9 KO hippocampus (1.1 ± 0.1 relatively to control; Figures 7B and 7C). As a control for epileptic activity, both WT and MMP9 KO mice exhibited upregulation of the activity-regulated protein Arc/Arg3.1 after PSE (Figure 7B).

Given the enrichment of NLG1-NTFs during the first postnatal weeks (Figures 2G and 2H), we addressed whether NLG1 cleavage is regulated by sensory experience during development. For this, we subjected mice to 5 days of dark rearing (DR) from P21–P26, a period of heightened sensory-evoked refinement of visual cortical circuits (Hensch, 2004), and subsequently re-exposed them to light for a brief period of 2 hr (DR+2hL, Figure 7D). This protocol induces rapid synaptic remodeling in the visual cortex and results in extensive molecular, functional, and structural synaptic changes (Philpot et al., 2001; Tropea et al., 2010). With this paradigm, 2 hr of re-exposure to light after 5 days of DR caused an increase in NLG1 cleavage in the visual cortex of WT mice (DR: 1.0 ± 0.1; DR+2hL: 1.5 ± 0.2, relatively to light-reared (LR) group; Figures 7E and 7F), but not in MMP9 KO animals (DR: 0.9 ± 0.1; DR+2hL: 1.0 ± 0.1; relative to LR group). Together these findings indicate that increased neuronal activity in vivo triggers MMP9-dependent cleavage of NLG1 in both mature and developing circuits.

DISCUSSION

Cleavage and Loss of Neuroligin-1 from Synapses

Although implicated in diverse forms of activity-dependent synaptic maturation and plasticity (Choi et al., 2011; Chubykin et al., 2007; Jung et al., 2010), it has been unclear whether neuroligins acutely regulate synapse function and whether the neuroligin-neurexin transsynaptic complex undergoes dynamic dissociation. Here we have shown that increased neuronal activity decreases synaptic NLG1 in minutes. MMP inhibitors, but not lysosome or proteasome inhibitors, block this effect, indicating that, under these conditions, NLG1 is predominantly regulated by MMP proteolytic cleavage (Figures 1G and 1H). The extent of endogenous NLG1 loss from synapses observed using biochemical methods is greater than that observed by immunostaining (Figure 1). This disparity may be attributed to the broad specificity of the pan-NLG antibody used for immunolabeling and to the fact that it targets the C-terminal domain of NLGs, an epitope that is further regulated by the γ-secretase complex (Figures S3E and S3F). It will be important to address how other NLG isoforms are regulated by MMPs and whether NLG1-CTFs participate in intracellular signaling.

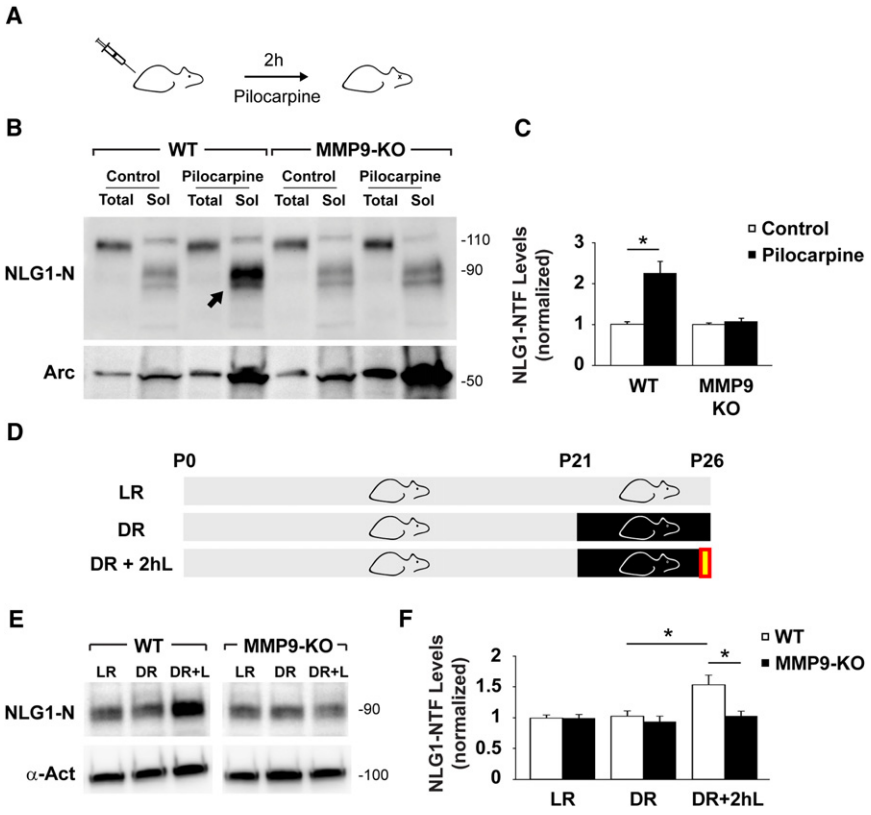

Figure 7. NLG1 Cleavage Is Triggered by Neural Activity and Sensory Experience In Vivo

(A) WT and MMP9 KO mice were injected with pilocarpine (315 mg/kg) or saline (control) for 2 hr.

(B) Immunoblot analysis of total extracts (5 μg) and soluble fractions (Sol, 50 μg) of hippocampi from mice injected with pilocarpine or saline (control). Arrow indicates increased NLG1-NTFs after PSE in WT mice.

(C) Means ± SEMs of NLG1-NTFs levels in indicated conditions normalized to control. n = 9 animals in each WT group; n = 10 and 11 in MMP9 KO control and pilocarpine groups, respectively. *$p < 0.005$.

(D) WT and MMP9-KO mice were reared in a normal 12 hr day/night cycle (LR) for 26 days or submitted to dark rearing for 5 days from P21–P26 (DR). DR+2hL indicates group submitted to 2 hr light exposure (yellow box) after DR.

(E) Immunoblot analysis of primary visual cortex soluble fractions of P26 mice reared under different conditions. α-actinin (α-Act) was used as a loading control.

(F) Means ± SEM of NLG1-NTFs levels under different conditions normalized to LR groups. n = 27 animals in each WT group; n = 24, 25, and 28 animals in MMP9 KO LR, DR, and DR+2hL groups, respectively. *$p < 0.01$.

Multiple soluble NLG1-NTF species can be detected in the brain (Figure 2D), suggesting that NLG1 contains more than one cleavage site. This observation provides a plausible explanation for why single amino acid point mutations in the juxtamembrane region of NLG1 fail to prevent MMP-dependent cleavage, which instead requires substitution of a 24 amino acid segment (Figures 4A and 4B). Moreover, basal levels of NLG1-NTFs can be detected in brain extracts from MMP9 KO mice (Figure 7B), indicating the existence of MMP9-independent mechanisms cleaving NLG1. In addition, our data indicate that NLG1-NTFs are most abundant during the first postnatal weeks (Figures 2G and 2H), suggesting that NLG1 cleavage may have different functions during development. It will be important to define in detail the activity-independent and MMP9-independent mechanisms of NLG1 cleavage and their specific role in synapse development and plasticity. Nevertheless, our results indicate that MMP9 is required for activity-dependent cleavage of NLG1 in multiple cellular contexts in vivo (Figure 7) and in vitro (Figures 3 and 4), consistent with the known involvement of MMP9 in multiple forms of synaptic plasticity (Bozdagi et al., 2007; Nagy et al., 2006; Szklarczyk et al., 2002; Wang et al., 2008; Wilczynski et al., 2008).

Focal uncaging of glutamate triggers MMP9-dependent cleavage of postsynaptic NLG1, indicating that this mechanism is regulated locally (Figures 4C and 4J). Interestingly, we detected a small heterosynaptic decrease of GFP-NLG1 from neighboring dendritic spines after synaptic stimulation (Figures 4C and 4J), suggesting that MMP9 activation may spread to adjacent dendritic regions. It remains unclear how NMDAR/CaMK signaling couples to MMP9 activity; however, considering the presence of MMP9 in spino-dendritic tubulovesicular structures (Wilczynski et al., 2008), one possibility is that CaMK activation triggers exocytosis of MMP9-containing vesicles in nearby dendritic regions or spines (Kennedy and Ehlers, 2011). It will be interesting to address if persistent cleavage of NLG1 can induce dendrite-wide effects and how the surface pools of NLGs are redistributed and replenished following periods of increased MMP-9 activity.

Neuroligin Cleavage as a Transsynaptic Retrograde Signal

Acute ectodomain cleavage of postsynaptic NLG1 causes rapid loss of NRX1β from apposing presynaptic terminals (Figures 5C, 5E, and 5G). The presynaptic protein synaptophysin is not affected by NLG1 cleavage, indicating that shedding of NLG1 is not accompanied by gross structural changes in presynaptic terminals (Figures 5D and 5F). Considering the expanding set of transsynaptic NRX binding partners, these results suggest that postsynaptic NLG1 is an important regulator of NRX1β stability at synapses. Previous studies have shown that deletion of αNRXs in mice reduces action-potential-evoked neurotransmitter release due to impaired presynaptic Ca^{2+} channel function (Missler et al., 2003). However, due to the role of NRXs in synapse maturation, it has been unclear whether this effect is due to indirect developmental effects or reflects an ongoing role of NRXs in neurotransmitter release. Using the

highly selective thrombin-induced cleavage of NLG1, we show an overall reduction in excitatory transmission and release probability concurrent with NRX1β loss (Figure 6). These findings support the notion that the NLG-NRX complex is a critical regulator of neurotransmitter release (Futai et al., 2007; Missler et al., 2003; Zhang et al., 2005) and provide evidence that NLG1-dependent regulation of presynaptic function can occur over time scales of minutes.

In mature hippocampal and cortical cultures, postsynaptic receptor blockade increases mEPSC frequency (Burrone et al., 2002; Thiagarajan et al., 2005; Wierenga et al., 2006) and augments presynaptic terminal size and release probability (Murthy et al., 2001; Thiagarajan et al., 2005). By contrast, local stimulation of dendrites acutely reduces release probability of contacting presynaptic terminals (Branco et al., 2008). These data have implied the existence of local transsynaptic negative feedback signals capable of modifying presynaptic function based on postsynaptic activity. Our results indicate that NLG1 cleavage is bidirectionally regulated by activity (Figures 3A and 3B). Moreover, acute NLG1 cleavage decreases release probability, whereas expression of a cleavage-resistant NLG1 isoform induces the opposite effect (Figure 6). Together, these data support a model where increased or decreased local NLG1 cleavage alternately dampens or augments presynaptic function based on postsynaptic activity, thereby contributing to overall levels of neuronal excitability.

MMP9-Dependent Cleavage of Neuroligin-1 in Development and Disease

The developmental profile of NLG1-NTFs in the brain (Figures 2G and 2H) indicates that NLG1 cleavage is upregulated during early stages of development, a time when activity-dependent mechanisms sculpt new circuits (Hensch, 2004). Moreover, our results indicate that MMP9-dependent cleavage of NLG1 is regulated by sensory experience during visual cortex maturation (Figures 7E and 7F). Interestingly, tissue plasminogen activator, a robust activator of MMP9 (Wang et al., 2003), regulates synapse maintenance during cortical development (Mataga et al., 2004), whereas MMP9 inhibition accelerates spine maturation in cultures (Bilousova et al., 2009). It will be interesting to address if NLG1 cleavage is involved in the activity-dependent mechanisms underlying synaptic maturation during development.

In addition, MMP9-dependent cleavage of NLG1 is increased during status epilepticus in the hippocampus of adult mice, indicating that this mechanism occurs in vivo not only during development, but also in mature circuits. Interestingly, MMP9 is upregulated and activated during seizures and, in turn, induces extensive synaptic plasticity and remodeling of hippocampal circuits (Szklarczyk et al., 2002; Wilczynski et al., 2008). Although our results indicate that postsynaptic structure and function remain largely unaffected following NLG1 cleavage (Figures 5A, 5B, and 5F; Movie S1), it remains to be determined whether further processing or long-term loss of NLG1 can impact postsynaptic function and stability. Finally, several NLG and NRX mutations have been linked to autism spectrum disorders (ASDs) (Südhof, 2008). In humans, ASDs emerge during the first years of infancy and are often associated with epileptic disorders. Our results implicate NLG1 cleavage with epileptiform activity and maturation of developing neuronal circuits. The acute proteolytic regulation of neuroligins reported here may provide novel insight into the pathophysiological mechanisms and therapeutic strategies for synaptic dysfunction in ASDs. More broadly, such a mechanism may provide a general paradigm for transsynaptic signaling in diverse neural circuits.

EXPERIMENTAL PROCEDURES

DNA Constructs and Antibodies

PSD95-mCh was a gift from Thomas Blanpied (University of Maryland). mCherry-N1 vector was a gift from Roger Tsien (University of California, San Diego). Rat GFP-NLG1 in pcDNA3 (ΔA splice variant) was kindly provided by Ann Marie Craig (University of British Columbia), and NRX1β-mCh was a gift from Thomas Südhof (Stanford University). Antibodies are listed in Supplemental Experimental Procedures.

Biochemical Analysis of Brain, Whole Cell Extracts, and PSD Fractions

Whole cell, synaptic plasma membrane, and PSD fractions from high density neuronal cultures were prepared and analyzed as described previously (Ehlers, 2003).

Surface Biotinylation and Isolation of Soluble Cleavage Products

Biotinylation-based internalization assays was performed as described previously (Ehlers, 2000). For isolation of soluble cleavage products, DIV21 cortical cultures were incubated in PBS/Ca^{2+} with 1 mg/ml Sulfo-LC-Biotin-NHS (Pierce) for 10 min at 37°C. Cultures were washed in PBS/Ca^{2+} with 10 mM Tris (pH 7.4), rinsed 2× in PBS/Ca^{2+}, and incubated in conditioned media at 37°C for the indicated time period. Pharmacological inhibitors were added 5 min prior to manipulations of neuronal activity. After incubation, culture media was collected, supplemented with protease inhibitors (Roche), and centrifuged at 16,000 × *g* for 20 min. For surface-labeled controls, cultures were washed 2× with PBS/Ca^{2+}, immediately lysed with precipitation buffer (PBS with 1% Triton X-100, 5 mM EDTA, 10 mM L-lysine [pH 7.4]), sonicated, and centrifuged at 16,000 × *g* for 20 min. Supernatants were incubated overnight with 50 μl NeutrAvidin Plus UltraLink Resin (Pierce) at 4°C. For NMDA stimulation, cells were incubated in media containing 50 μM NMDA for 5 min and subsequently incubated in conditioned media for 2 hr. Both media samples were pooled before streptavidin precipitation. For all samples, precipitated proteins were boiled in 2× sample buffer and resolved by SDS-PAGE prior to immunoblot analysis. For APMA experiments, 50 mM APMA stock was solubilized in 0.1 N NaOH and added at a final concentration of 0.5 mM to culture media, together with 10 mM 4-(2-hydroxyethyl)-1-piperazineethanesulfonic acid (HEPES) (pH 7.4).

In Utero Electroporation

E15.5 timed-pregnant C57BL/6 mice were anesthetized by 2% isoflurane. Uterine horns were gently mobilized from the peritoneal cavity and 1 μg/μl of GFP-NLG1 or GFP-NLG1-ΔSD3, and tdTomato cDNAs were injected into the lateral ventricle of the left hemisphere of intrauterine embryos using an ~50-μm-diameter pipette sharply beveled at 15°–20° (Narishige, Japan). DNA was transfected with five electrical pulses with a 1 s interval (50 V, 50 ms) (CUY21 electroporator, NEPA GENE, Japan).

Slice Culture Preparation

Organotypic hippocampal slice cultures were prepared from 8-day-old mice and cut with ~400 μm thickness. Three to five slices were placed in a sterile culture plate insert (Millicell-CM, Millipore). DNA constructs were biolistically transfected with a Helios Gene Gun (Biorad) 2 days later.

Two-Photon Microscopy and Glutamate Uncaging

Uncaging of MNI-glutamate and spine/dendrite imaging were performed using a custom-built microscope combining two-photon laser-scanning microscopy and two-photon laser photoactivation, as previously described (Kwon and Sabatini, 2011). Organotypic or acute brain slices were placed in a slice chamber perfused with normal artificial cerebrospinal fluid containing (in mM) 127 NaCl, 2.5 KCl, 25 $NaHCO_3$, 1.25 NaH_2PO_4, 2 $CaCl_2$, 1 $MgCl_2$, and 25 glucose. Dendrite/spine images were acquired with 840 nm excitation wavelength, and photolysis of MNI-glutamate was performed by focal illumination with 720 nm light. The laser power arriving at the specimen (10∼15 mW) was controlled by Pockels cells (Conoptics, Danbury, CT). Uncaging was done ∼1 μm away from the spine head and 80 laser pulses (4 ms) were delivered at 2 Hz. Spine/dendrite image stacks were taken immediately before and after the induction protocol (<1 min). To analyze changes of GFP-NLG1, green fluorescence (G) measured in the spine head or subjacent dendrite was normalized to the red signal (R) from the same area and changes in the G/R ratios compared before and after the induction protocol.

Confocal Imaging and FM4-64 Unloading Experiments

Confocal images of fixed samples and live cells were obtained using a Perkin Elmer Ultraview spinning disc confocal microscope with either a 40 × 1.3 N.A. objective or a 60 × 1.4 N.A. objective. For immunocytochemistry, DIV21 hippocampal neurons were fixed in 4% paraformaldehyde/4% sucrose in PBS for 20 min, permeabilized with 0.2% Triton X-100 for 15 min, and incubated with indicated antibodies. For live imaging, cells were imaged in E4 media containing (in mM) 10 HEPES, 120 NaCl, 3 KCl, 10 D-glucose, 2 $CaCl_2$, and 2 $MgCl_2$ at 37°C. Maximum projections of individual stacks were analyzed using Metamorph software (Universal Imaging Corporation). Results shown correspond to the average of all neurons per condition. Statistical significance was determined by unpaired t test, and error bars represent standard error of the means.

FM4-64 (10 μM) uptake was performed using 90 mM KCl loading media containing (in mM) 10 HEPES, 33 NaCl, 90 KCl, 10 D-glucose, 2 $CaCl_2$, 2 $MgCl_2$, 20 μM NBQX, and 50 μM APV for 1 min. Cells were washed three times in washing buffer (WB: E4 with 0.5 mM $CaCl_2$ and 10 mM $MgCl_2$) for 30 s, two times for 15 s in WB containing 1 mM ADVASEP-7 (Sigma), and three times in WB. FM4-64 fluorescence was acquired with 567 nm excitation and a 647 nm emission filter. GFP imaging was done at the end of each time lapse to minimize photobleaching. Unloading solution containing (in mM) 10 HEPES, 63 NaCl, 60 KCl, 10 D-glucose, 2 $CaCl_2$, 2 $MgCl_2$, 20 μM NBQX, and 50 μM APV was added with a precision of <2 s. Time constants (τ) of FM4-64 fluorescence decay at boutons corresponding to each condition were pooled and analyzed by a Kolmogorov-Smirnov test. Statistical significance was determined using unpaired t tests. For more details, see Supplemental Experimental Procedures.

Electrophysiological Recordings

EPSC internal solution contained (in mM) 30 $CsSO_4$, 70 K_2SO_4, 25 HEPES, 25 N-methyl-D-glucamine, 0.1 $CaCl_2$, 1 EGTA, 2 (Na)ATP, and 0.1 leupeptin (pH 7.2), ∼300 mOsm, and EPSC external solution contained (in mM) 150 NaCl, 5 KCl, 10 HEPES, 1 $MgCl_2$, 30 D-glucose, 2 $CaCl_2$, and 30 μM bicuculline. Only cells with series resistance <30 MΩ and <20% change in input resistance, series resistance, and holding current were analyzed. EPSCs were evoked with a concentric bipolar stimulating electrode (200 μs pulse duration). Paired-pulse responses (100 ms interval) were evoked every 30 s by stimulation of nearby cells. For mEPSC recordings, external solution contained additional 1 μM TTX. mIPSC internal solution contained (in mM) 150 KCl, 3 $MgCl_2$, 15 HEPES, 0.1 $CaCl_2$, 1 EGTA, 2 Na_2ATP, and 0.1 leupeptin [pH 7.2], ∼300 mOsm. mIPSC external solution contained 1 μM TTX, 50 μM D-APV, and 10 μM CNQX instead of bicuculline. All currents were recorded at −70 mV voltage clamp.

Pilocarpine-Induced Status Epilepticus

P60 female FVB or FVB.Cg-*Mmp9*^{tm1Tvu}/J mice (∼18–25 g) were injected intraperitoneally (i.p.) with 1 mg/kg scopolamine methyl nitrate (Sigma) 30 min prior to the experiment. Status epilepticus was induced by i.p. injection of 315 mg/kg pilocarpine hydrochloride (Sigma), while controls were injected with vehicle alone (sterile 0.9% NaCl). The experiment was terminated 2 hr later, and hippocampal tissue was collected and flash frozen. Only animals with class IV or higher seizures were used for analysis.

Dark Rearing Experiments

Male and female FVB or FVB.Cg-*Mmp9*^{tm1Tvu}/J mice were reared in a normal light dark cycle (12 hr light/12 hr dark) from birth until P26 (LR) or were transferred to a dark room in complete darkness at P21 (DR). The DR+2hL group was re-exposed to light for 2 hr before euthanization. The primary visual cortex was extracted and homogenized as described previously (Philpot et al., 2001).

SUPPLEMENTAL INFORMATION

Supplemental Information includes six figures, Supplemental Experimental Procedures, and two movies and can be found with this article online at http://dx.doi.org/10.1016/j.neuron.2012.07.006.

ACKNOWLEDGMENTS

We thank Susana da Silva for technical assistance and data analysis. We thank Susana da Silva, Ian Davison, Cyril Hanus, Juliet Hernandez, Hyun-Soo Je, and Thomas Newpher for review of the manuscript. We thank Irina Lebedeva, Marguerita Klein, Sarah Lancaster, and Jaya Miriyala for excellent technical assistance. We thank Nils Brose for providing NLG1-KO mouse brains. Work in the laboratory of M.D.E. was supported by HHMI and grants from NIMH-NIH, NINDS-NIH, and the Simons Foundation. Work in the laboratory of B.D.P. is supported by grants from NEI-NIH and the Simons Foundation. R.T.P. was supported by the Portuguese FCT grant SFRH/BD/15217/2004. P.A.K. was supported by NICHD training Grant T32HD040127.

Accepted: July 3, 2012
Published: September 5, 2012

REFERENCES

Bilousova, T.V., Dansie, L., Ngo, M., Aye, J., Charles, J.R., Ethell, D.W., and Ethell, I.M. (2009). Minocycline promotes dendritic spine maturation and improves behavioural performance in the fragile X mouse model. J. Med. Genet. *46*, 94–102.

Bozdagi, O., Nagy, V., Kwei, K.T., and Huntley, G.W. (2007). In vivo roles for matrix metalloproteinase-9 in mature hippocampal synaptic physiology and plasticity. J. Neurophysiol. *98*, 334–344.

Branco, T., Staras, K., Darcy, K.J., and Goda, Y. (2008). Local dendritic activity sets release probability at hippocampal synapses. Neuron *59*, 475–485.

Burrone, J., O'Byrne, M., and Murthy, V.N. (2002). Multiple forms of synaptic plasticity triggered by selective suppression of activity in individual neurons. Nature *420*, 414–418.

Chih, B., Engelman, H., and Scheiffele, P. (2005). Control of excitatory and inhibitory synapse formation by neuroligins. Science *307*, 1324–1328.

Chih, B., Gollan, L., and Scheiffele, P. (2006). Alternative splicing controls selective trans-synaptic interactions of the neuroligin-neurexin complex. Neuron *51*, 171–178.

Choi, Y.B., Li, H.L., Kassabov, S.R., Jin, I., Puthanveettil, S.V., Karl, K.A., Lu, Y., Kim, J.H., Bailey, C.H., and Kandel, E.R. (2011). Neurexin-neuroligin transsynaptic interaction mediates learning-related synaptic remodeling and long-term facilitation in aplysia. Neuron *70*, 468–481.

Chubykin, A.A., Atasoy, D., Etherton, M.R., Brose, N., Kavalali, E.T., Gibson, J.R., and Südhof, T.C. (2007). Activity-dependent validation of excitatory versus inhibitory synapses by neuroligin-1 versus neuroligin-2. Neuron *54*, 919–931.

Dahlhaus, R., Hines, R.M., Eadie, B.D., Kannangara, T.S., Hines, D.J., Brown, C.E., Christie, B.R., and El-Husseini, A. (2010). Overexpression of the cell adhesion protein neuroligin-1 induces learning deficits and impairs synaptic plasticity by altering the ratio of excitation to inhibition in the hippocampus. Hippocampus *20*, 305–322.

Dalva, M.B., McClelland, A.C., and Kayser, M.S. (2007). Cell adhesion molecules: signalling functions at the synapse. Nat. Rev. Neurosci. *8*, 206–220.

Dean, C., Scholl, F.G., Choih, J., DeMaria, S., Berger, J., Isacoff, E., and Scheiffele, P. (2003). Neurexin mediates the assembly of presynaptic terminals. Nat. Neurosci. *6*, 708–716.

Ehlers, M.D. (2000). Reinsertion or degradation of AMPA receptors determined by activity-dependent endocytic sorting. Neuron *28*, 511–525.

Ehlers, M.D. (2003). Activity level controls postsynaptic composition and signaling via the ubiquitin-proteasome system. Nat. Neurosci. *6*, 231–242.

Ethell, I.M., and Ethell, D.W. (2007). Matrix metalloproteinases in brain development and remodeling: synaptic functions and targets. J. Neurosci. Res. *85*, 2813–2823.

Etherton, M.R., Tabuchi, K., Sharma, M., Ko, J., and Südhof, T.C. (2011). An autism-associated point mutation in the neuroligin cytoplasmic tail selectively impairs AMPA receptor-mediated synaptic transmission in hippocampus. EMBO J. *30*, 2908–2919.

Futai, K., Kim, M.J., Hashikawa, T., Scheiffele, P., Sheng, M., and Hayashi, Y. (2007). Retrograde modulation of presynaptic release probability through signaling mediated by PSD-95-neuroligin. Nat. Neurosci. *10*, 186–195.

Gottmann, K. (2008). Transsynaptic modulation of the synaptic vesicle cycle by cell-adhesion molecules. J. Neurosci. Res. *86*, 223–232.

Graf, E.R., Zhang, X., Jin, S.X., Linhoff, M.W., and Craig, A.M. (2004). Neurexins induce differentiation of GABA and glutamate postsynaptic specializations via neuroligins. Cell *119*, 1013–1026.

Gutiérrez, R.C., Flynn, R., Hung, J., Kertesz, A.C., Sullivan, A., Zamponi, G.W., El-Husseini, A., and Colicos, M.A. (2009). Activity-driven mobilization of postsynaptic proteins. Eur. J. Neurosci. *30*, 2042–2052.

Heine, M., Thoumine, O., Mondin, M., Tessier, B., Giannone, G., and Choquet, D. (2008). Activity-independent and subunit-specific recruitment of functional AMPA receptors at neurexin/neuroligin contacts. Proc. Natl. Acad. Sci. USA *105*, 20947–20952.

Hensch, T.K. (2004). Critical period regulation. Annu. Rev. Neurosci. *27*, 549–579.

Ichtchenko, K., Hata, Y., Nguyen, T., Ullrich, B., Missler, M., Moomaw, C., and Südhof, T.C. (1995). Neuroligin 1: a splice site-specific ligand for beta-neurexins. Cell *81*, 435–443.

Jung, S.Y., Kim, J., Kwon, O.B., Jung, J.H., An, K., Jeong, A.Y., Lee, C.J., Choi, Y.B., Bailey, C.H., Kandel, E.R., and Kim, J.H. (2010). Input-specific synaptic plasticity in the amygdala is regulated by neuroligin-1 via postsynaptic NMDA receptors. Proc. Natl. Acad. Sci. USA *107*, 4710–4715.

Kennedy, M.J., and Ehlers, M.D. (2011). Mechanisms and function of dendritic exocytosis. Neuron *69*, 856–875.

Ko, J., Zhang, C., Arac, D., Boucard, A.A., Brunger, A.T., and Südhof, T.C. (2009). Neuroligin-1 performs neurexin-dependent and neurexin-independent functions in synapse validation. EMBO J. *28*, 3244–3255.

Kwon, H.B., and Sabatini, B.L. (2011). Glutamate induces de novo growth of functional spines in developing cortex. Nature *474*, 100–104.

Levinson, J.N., Chéry, N., Huang, K., Wong, T.P., Gerrow, K., Kang, R., Prange, O., Wang, Y.T., and El-Husseini, A. (2005). Neuroligins mediate excitatory and inhibitory synapse formation: involvement of PSD-95 and neurexin-1beta in neuroligin-induced synaptic specificity. J. Biol. Chem. *280*, 17312–17319.

Lisman, J.E., and Harris, K.M. (1993). Quantal analysis and synaptic anatomy—integrating two views of hippocampal plasticity. Trends Neurosci. *16*, 141–147.

Mataga, N., Mizuguchi, Y., and Hensch, T.K. (2004). Experience-dependent pruning of dendritic spines in visual cortex by tissue plasminogen activator. Neuron *44*, 1031–1041.

Michaluk, P., Mikasova, L., Groc, L., Frischknecht, R., Choquet, D., and Kaczmarek, L. (2009). Matrix metalloproteinase-9 controls NMDA receptor surface diffusion through integrin beta1 signaling. J. Neurosci. *29*, 6007–6012.

Missler, M., Zhang, W., Rohlmann, A., Kattenstroth, G., Hammer, R.E., Gottmann, K., and Südhof, T.C. (2003). Alpha-neurexins couple Ca2+ channels to synaptic vesicle exocytosis. Nature *423*, 939–948.

Murthy, V.N., Schikorski, T., Stevens, C.F., and Zhu, Y. (2001). Inactivity produces increases in neurotransmitter release and synapse size. Neuron *32*, 673–682.

Nagy, V., Bozdagi, O., Matynia, A., Balcerzyk, M., Okulski, P., Dzwonek, J., Costa, R.M., Silva, A.J., Kaczmarek, L., and Huntley, G.W. (2006). Matrix metalloproteinase-9 is required for hippocampal late-phase long-term potentiation and memory. J. Neurosci. *26*, 1923–1934.

Philpot, B.D., Sekhar, A.K., Shouval, H.Z., and Bear, M.F. (2001). Visual experience and deprivation bidirectionally modify the composition and function of NMDA receptors in visual cortex. Neuron *29*, 157–169.

Restituito, S., Khatri, L., Ninan, I., Mathews, P.M., Liu, X., Weinberg, R.J., and Ziff, E.B. (2011). Synaptic autoregulation by metalloproteases and γ-secretase. J. Neurosci. *31*, 12083–12093.

Scheiffele, P., Fan, J., Choih, J., Fetter, R., and Serafini, T. (2000). Neuroligin expressed in nonneuronal cells triggers presynaptic development in contacting axons. Cell *101*, 657–669.

Shipman, S.L., Schnell, E., Hirai, T., Chen, B.S., Roche, K.W., and Nicoll, R.A. (2011). Functional dependence of neuroligin on a new non-PDZ intracellular domain. Nat. Neurosci. *14*, 718–726.

Stan, A., Pielarski, K.N., Brigadski, T., Wittenmayer, N., Fedorchenko, O., Gohla, A., Lessmann, V., Dresbach, T., and Gottmann, K. (2010). Essential cooperation of N-cadherin and neuroligin-1 in the transsynaptic control of vesicle accumulation. Proc. Natl. Acad. Sci. USA *107*, 11116–11121.

Südhof, T.C. (2008). Neuroligins and neurexins link synaptic function to cognitive disease. Nature *455*, 903–911.

Szklarczyk, A., Lapinska, J., Rylski, M., McKay, R.D., and Kaczmarek, L. (2002). Matrix metalloproteinase-9 undergoes expression and activation during dendritic remodeling in adult hippocampus. J. Neurosci. *22*, 920–930.

Thiagarajan, T.C., Lindskog, M., and Tsien, R.W. (2005). Adaptation to synaptic inactivity in hippocampal neurons. Neuron *47*, 725–737.

Tropea, D., Majewska, A.K., Garcia, R., and Sur, M. (2010). Structural dynamics of synapses in vivo correlate with functional changes during experience-dependent plasticity in visual cortex. J. Neurosci. *30*, 11086–11095.

Van Wart, H.E., and Birkedal-Hansen, H. (1990). The cysteine switch: a principle of regulation of metalloproteinase activity with potential applicability to the entire matrix metalloproteinase gene family. Proc. Natl. Acad. Sci. USA *87*, 5578–5582.

Varoqueaux, F., Aramuni, G., Rawson, R.L., Mohrmann, R., Missler, M., Gottmann, K., Zhang, W., Südhof, T.C., and Brose, N. (2006). Neuroligins determine synapse maturation and function. Neuron *51*, 741–754.

Wang, X., Lee, S.R., Arai, K., Lee, S.R., Tsuji, K., Rebeck, G.W., and Lo, E.H. (2003). Lipoprotein receptor-mediated induction of matrix metalloproteinase by tissue plasminogen activator. Nat. Med. *9*, 1313–1317.

Wang, X.B., Bozdagi, O., Nikitczuk, J.S., Zhai, Z.W., Zhou, Q., and Huntley, G.W. (2008). Extracellular proteolysis by matrix metalloproteinase-9 drives dendritic spine enlargement and long-term potentiation coordinately. Proc. Natl. Acad. Sci. USA *105*, 19520–19525.

Wierenga, C.J., Walsh, M.F., and Turrigiano, G.G. (2006). Temporal regulation of the expression locus of homeostatic plasticity. J. Neurophysiol. *96*, 2127–2133.

Wilczynski, G.M., Konopacki, F.A., Wilczek, E., Lasiecka, Z., Gorlewicz, A., Michaluk, P., Wawrzyniak, M., Malinowska, M., Okulski, P., Kolodziej, L.R., et al. (2008). Important role of matrix metalloproteinase 9 in epileptogenesis. J. Cell Biol. *180*, 1021–1035.

Wittenmayer, N., Körber, C., Liu, H., Kremer, T., Varoqueaux, F., Chapman, E.R., Brose, N., Kuner, T., and Dresbach, T. (2009). Postsynaptic Neuroligin1 regulates presynaptic maturation. Proc. Natl. Acad. Sci. USA *106*, 13564–13569.

Yong, V.W. (2005). Metalloproteinases: mediators of pathology and regeneration in the CNS. Nat. Rev. Neurosci. *6*, 931–944.

Zhang, W., Rohlmann, A., Sargsyan, V., Aramuni, G., Hammer, R.E., Südhof, T.C., and Missler, M. (2005). Extracellular domains of alpha-neurexins participate in regulating synaptic transmission by selectively affecting N- and P/Q-type Ca2+ channels. J. Neurosci. *25*, 4330–4342.